Geomechanics and Engineering, *Vol. 30, No. 5 (2022) 471-478*
https://doi.org/10.12989/gae.2022.30.5.471

Changes in bound water and microstructure during consolidation creep of Guilin red clay

Dajin Zhang[1a], Guiyuan Xiao*[1,2], Le Yin[3], Guangli Xu[2] and Jian Wang[1]

[1]*Key Laboratory of Geotechnics of Guangxi, Guilin University of Technology, 541004, China*
[2]*School of Engineering, China University of Geosciences, Wuhan 430000, China*
[3]*The Guangxi Zhuang Autonomous Region Company of China National Tobacco Corporation, China*

(*Received June 11, 2022, Revised August 15, 2022, Accepted August 16, 2022*)

Abstract. Creep of soils has a significant impact on mechanical properties. The one-dimensional consolidation creep test, thermal analysis test, scanning electron microscope (SEM) test, and mercury compression test were performed on Guilin red clay to study the changes in bound water and microstructure during the creep process of Guilin red clay. According to the results of the tests, only free and weakly bound water is discharged during the creep of Guilin red clay. When the consolidation pressure p is in the 12.5-400.0 kPa range, it is primarily the discharge of free water; when the consolidation pressure p is in the 800.0-1600.0 kPa range, the weakly bound water is converted to free water and discharged. After consolidation creep, the microstructure of soil changes from granular overhead contact structure to flat sheet-like stacking structure, with a decrease in the number of large and medium pores, an increase in the number of small and micro pores, and a decrease in the fractal dimension of pores. The creep process of red clay is the discharge of weakly bound water as well as the compression of large pores into small pores and the transition of soil particles from loose to dense.

Keywords: consolidation creep; microstructure; pore water; red clay; thermal analysis tests

1. Introduction

Red clay soils are widely distributed throughout the world (Ghiyas and Bagheripour 2020) and in China they are distributed mainly in karst-developed provinces such as Guangxi, Yunnan, and Guizhou, with low compressibility and high strength (Zhu *et al.* 2021). In many places in the distribution area, red clay soils are used directly as foundations, and the creep properties of red clay soils can produce engineering problems such as settlement and collapse on foundations, which can have adverse effects on engineering construction (Zhang *et al.* 2019). Therefore, it is of great engineering importance to study the creep of red clay soils.

Currently, many scholars have conducted extensive research on the physical and mechanical properties of soils and have obtained good results (An *et al.* 2022, Guo *et al.* 2021, Jin *et al.* 2021). Creep, as a rheological phenomenon of soils, is directly related to the safety of the project itself and the surrounding environment. (Tavenas *et al.* 1978) conducted drained and undrained triaxial tests on superconsolidated clay, and the test results showed that the creep deformation of superconsolidated clay can be divided into volume strain and shear strain. (Dahhaoui *et al.* 2022) studied the one-dimensional compressive creep variation of bentonite under temperature and suction and found that the creep behavior of bentonite under temperature can be divided into primary consolidation and secondary consolidation, and the creep behavior under suction is mainly controlled by structural viscosity. (Ibrahim *et al.* 2022) used a three-dimensional finite element method to investigate the creep deformation of soft clay under vertical drainage and the numerical analysis of the creep behavior of soft clay under precompression showed that the preload stress is the main factor affecting the increase of the secondary compression index. (Kamoun and Bouassida 2018) performed triaxial tests on clayey soils with different saturation and stress levels and found that the shear deformation increased with the increasing initial saturation and stress level of clay samples and the variation of axial creep strain was semi-logarithmic with time. (Kaczmarek *et al.* 2017) studied the creep strain of clay in drained triaxial tests using computerized microscopic imaging techniques and found that the creep process of clay can be divided into decreasing creep strain rate, transitional constant creep rate, and accelerated creep deformation. In addition, many scholars have established creep models to describe the creep properties of soils, and the commonly used models are the theoretical creep model, empirical creep model (Mesri *et al.* 1981, Singh and Mitchell 1968) and semiempirical creep model (Kaczmarek and Dobak 2017, Liingaard *et al.* 2004). The new empirical creep model established by (Long *et al.* 2021), compared with Burgers model and Singh-Mitchell model, has more model parameters. (Bi *et al.* 2022) proposed a power law model to represent the creep behavior of cohesive soils with different plasticity indices based on long-term monitoring data in the field and indoor test data. (Leoni *et al.* 2008) proposed an anisotropic creep

*Corresponding author, Professor
E-mail: xiaoguiyuangit@163.com
[a]Master

ISSN: 2005-307X (Print), 2092-6219 (Online)

Table 1 Basic physical parameters of Guangxi red clay

Name	Liquid limit W_L/%	Plastic limit W_p/%	Optimum moisture content W/%	Maximum dry density ρ_d/g·cm^{-3}	Specific gravity *Gs*	Porosity ratio *e*
Red clay	79.9	33.9	26.5	1.56	2.67	0.712

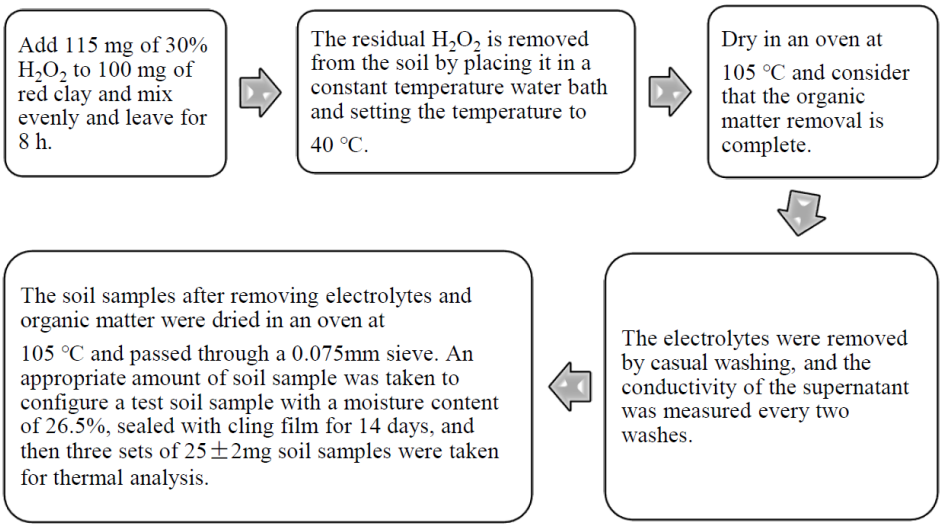

Fig. 1 Processing steps prior to red clay bound water testing

model for soft soils, which can study the directionality of creep in soft soils. (Zhu *et al*. 2021) established an equivalent cyclic creep model that can describe the cumulative cyclic deformation characteristics of soft clay soils by cyclic triaxial test tests. (Li and Kong 2021) used a modified stress-controlled triaxial apparatus to perform triaxial drainage compression tests on swelling soils and proposed a new non-linear creep model that can describe the creep characteristics of swelling soils. (Karim *et al.* 2011) developed an elastic-viscoplastic (EVP) model to analyze the stress-strain behavior of normally consolidated and superconsolidated clay soils over time.

Obviously, the creep properties of soils have been studied in depth by previous authors and abundant results have been obtained. However, these studies mainly focus on the influence of a certain variable on creep properties or derive the corresponding creep model based on the experimental results, but the derived model has limitations and cannot explain the nature of creep. Therefore, this paper takes Guilin red clay as the research object and obtains the pore water content in red clay by thermal analysis test. Combining with the one-dimensional consolidation creep test, scanning electron microscope test and mercury compression test, we quantitatively analyze the changes of bound water content and microstructure during the creep of red clay, aiming to explore the creep mechanism of red clay from two perspectives of bound water and microstructure.

2. Test materials and methods

2.1 Test materials

The red clay soil used in this test was taken from a site in Lingui District, Guilin City, Guangxi Province, which belongs to the solitary plain landscape, and the soil structure can be broadly divided into three layers: the first layer is a plain fill (Q_4^{ml}), with a layer thickness of 2.35-4.50 m; the second layer is a secondary red clay (Q_4^{dl}), reddish-brown, with a more homogeneous and fine texture, with a layer thickness of 1.35-4.50 m; the third layer is a pebble gravel soil (Q_4^{dl}), with a layer thickness of 1.00-5.35 m. The soil samples were taken from the second layer at a depth of 6.0-8.0 m. Air-dried soil samples were crushed and passed through a 2 mm geotechnical sieve. This batch of red clay had an air-dried moisture content of 3.66%, and the other basic physical parameters of the soil samples are shown in Table 1.

2.2 Solidification creep test program

The test apparatus was a pneumatic consolidator, and the soil samples were prepared following the relevant specifications of the Standard for Geotechnical Test Methods (GBT50123-2019) (MWR (China) 2019). Three parallel tests with six specimens were set up, wherein the specimens were always in a water-filled state throughout the test. The specimens were placed in the pneumatic consolidation apparatus as per the procedures of the standard consolidation test in the relevant specification, keeping the pressure levels 12.5 kPa→25.0 kPa→50.0 kPa→100.0 kPa→200.0 kPa→400.0 kPa→800.0 kPa→1600.0 kPa. The following loading level may be applied when the consolidation under each pressure level for 24 h or the hourly deformation was less than 0.01 mm (MWR (China) 2019).

2.3 Combined water testing program

The bound water content of red clay specimens is

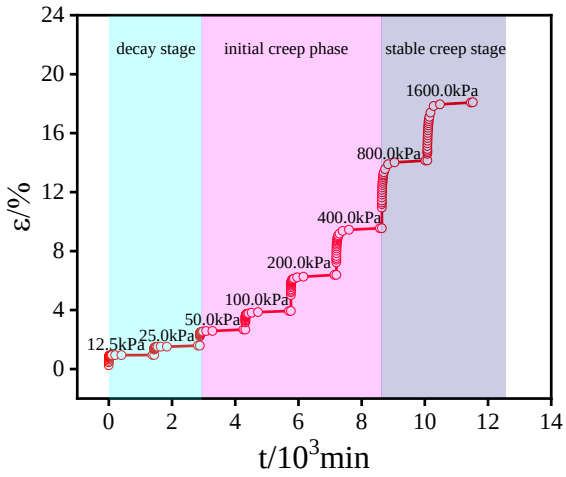

Fig. 2 Consolidation creep curve of red clay

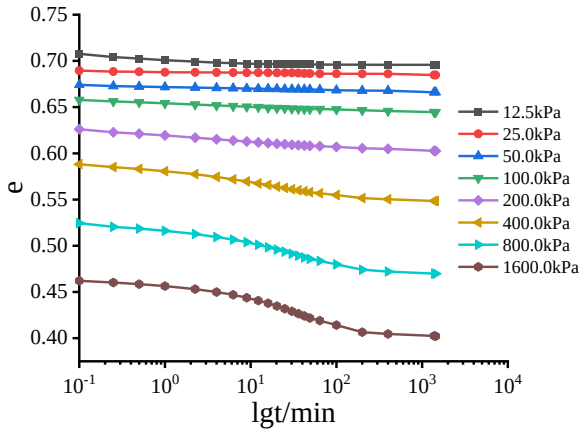

Fig. 3 *e*-lgt curves for each load level

determined using a thermal analysis test. The thermal analysis method works on the principle of using the different thermal effects that occur during the heating of clay minerals to differentiate between the various clay minerals. The STA8000 simultaneous analyzer with a temperature range of 25 to 400°C and a heating rate of 10 °C/min is used; the test gas is nitrogen, and the heat flow atmospheric flow rate is set at 20 mL/min. Because of the interference of electrolytes and organic matter in the soil, the soil sample is processed prior to testing to achieve better test results, as shown in Fig. 1.

2.4 Microstructure testing program

SEM was used to examine the microstructure of the specimens before and after solidification creep, and the photographs were processed using Image-Pro Plus image software to obtain microstructural parameters. The test procedure was as follows: three sets of specimens were selected before and after solidification creep and dried in a constant temperature chamber at 40°C. The preparation of SEM samples and the microstructural test methods were as per the available literature (Li *et al.* 2010).

As part of the test procedures, the specimen was chopped into 1 cm^3 pieces of soil with a fine steel wire and frozen in liquid nitrogen (–196°C) for 15 min. Further, the soil block was removed and placed in the freeze dryer to vacuum for 24 h to remove the moisture in the soil block. Finally, mercury compression tests were conducted on the dried soil blocks to determine the pore size distribution pattern.

3. Test results and analysis

3.1 Creep test results

Fig. 2 shows the creep test results of the red clay, wherein the creep curve of the red clay soil is separated into the decay phase, the initial creep phase, and the stable creep phase. The decay stage is characterized by a low load, with p=12.5 kPa-25.0 kPa, which develops the creep of the soil resulting in a final speed of zero. During the initial creep stage, the creep deformation of the soil is minimal and quickly stable with p=50.0 kPa-400 kPa, wherein the creep deformation increases continuously with time to reach p=800.0 kPa-1600.0 kPa, to stabilize the creep curve. This stage with constant creep deformation rate and is called the stable creep stage.

Fig. 3 shows the *e*-lgt curves of red clay under different loads, depicting the relationship between the shape of the *e*-lgt curve and the size of the load. The shape of the *e*-lgt curve is approximately a gentle straight line for low loads with p=12.5 kPa-100.0 kPa, while it appears segmented with increased load. The e-lgt curve is characterized by an inverse '*S*' shape in the front section and a gentle straight line in the tail section. The segmentation phenomenon is more apparent with larger loads. The *e*-lgt curve is divided into primary and secondary consolidation (Gao 2019), of saturated soil represented by an inverse "*S*" shape and the gentle straight line at the end. The slope of the gentle straight line at the end is the secondary consolidation coefficient C_a, which is directly proportional to the creep deformation of the soil. Fig. 4 shows the sub consolidation coefficient variation curve with load for red clay soil calculated according to Eq. (1). The visibility of change in the coefficient of sub consolidation of red clay with the load reaches the maximum at p=800 kPa, followed by a decline and leveling off with an increase in load due to rearrangement of soil particles after stabilization and the relatively less increase in deformation with an increase in pressure.

$$C_{\mathrm{a}} = -\frac{\Delta e}{\Delta \lg(t)} \tag{1}$$

Where: 'e' is the pore ratio and 't' is time.

3.2 Binding water test results

The TG curve of the red clay was generated based on the thermal analysis test data to represent the percentage weight loss mass of the sample versus temperature T. In contrast, the DTG curve depicts the temperature inflection points of free and bound water of the test soil sample representing the amount of bound water in the soil and is

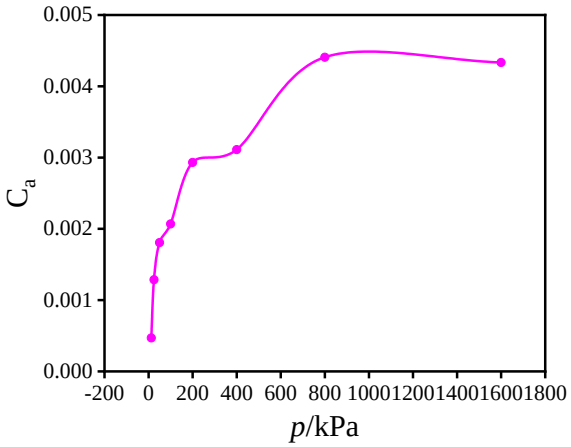

Fig. 4 Variation of consolidation coefficient at different consolidation pressures

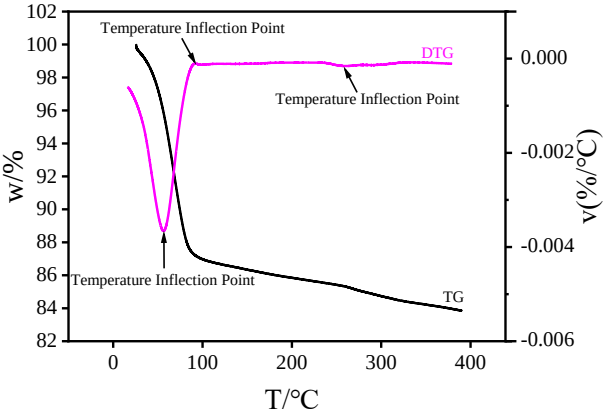

Fig. 5 TG-DTG curve of red clay

the first-order micro quotient of the TG curve versus time. Fig. 5 shows a plot of the TG-DTG curve for red clay soil.

Three distinct temperature inflection points can be seen on the DTG curve, as shown in Fig. 5, which is consistent with the findings of Xie *et al.* (2013), wherein the types of bound water in clay were determined using thermal analysis tests demonstrating the acceptance of the DTG curves in representing temperature inflection points of free water and bound water. The three temperature inflection points on the DTG curve represent the three weight-loss stages of the samples, with the temperature ranging from 26.32°C to 67.39°C, 67.39°C to 103.95°C and 103.95°C to 275.00°C, respectively. Free water, weakly bound water, and strongly bound water are the three types of water lost in the soil corresponding to the TG curves, with respective water contents of W_f=7.72%, W_0=5.42% and W_g=1.85%.

3.3 Changes in bound water content during creep

The soil sample is saturated by evacuation before the consolidation creep test, keeping fully saturated with free water and bound water throughout the test. Under the load, the pores are continuously compressed with a constant total particle volume V_s. The discharge patterns of free water, weakly bound water, and firmly bound water during the creep of red clay can be analyzed based on the change of

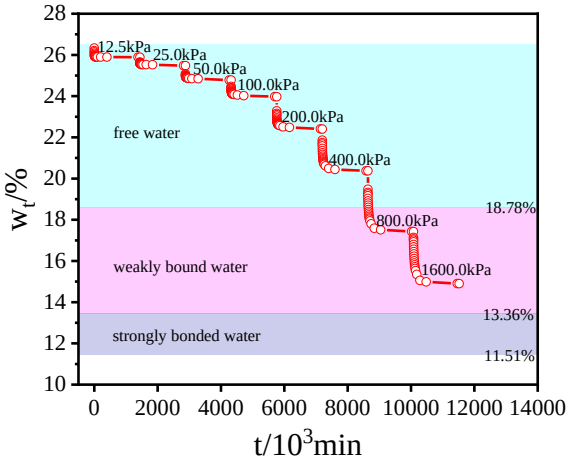

Fig. 6 Curves of water release processes in red clay during consolidation creep

soil pore ratio. The pore ratios of weakly bound water and strongly bound water at the beginning of the discharge are determined using the following Eq. (2).

$$\left.\begin{aligned} e_0 &= e - e\frac{w_f m_s}{\rho_{wt} V_w} = e - \frac{w_f \rho_s}{\rho_{wt}} \\ e_1 &= e\frac{w_g m_s}{\rho_{we} V_W} = \frac{w_g \rho_s}{\rho_{we}} \end{aligned}\right\} \tag{2}$$

Where: m_s is the total mass of solid particles in the soil; V_w is the volume of water in the soil; ρ_{wt} is the density of free water, (1.0 g/cm^3); ρ_{we} is the density of weakly bound water, taken as (1.3 g/cm^3) (Wu 1984); e_0 is the pore ratio at the start of draining of the weakly bound water; e_1 is the pore ratio when the strongly bound water starts to drain.

This corresponds to an e_0 of 0.501 and e_1 of 0.039. The water content of the soil during the creep can be estimated using Eq. (3), which is as follows.

$$w_t = \frac{m_w - m_t}{m_s} = \frac{m_w - \rho_w(e - e_t)V_s}{\rho_s V_s} \tag{3}$$

Where: m_w is the mass of water in the soil; m_t is the mass of water discharged from the soil sample at time t; e_t is the pore ratio of the soil sample at time t; ρ_w is the density of the water during the compression of the soil. This leads to Eq. (4), which is as follows.

$$w_t = \begin{cases} w - \frac{\rho_{wt}(e-e_t)}{\rho_s} & (e_t > e_1) \\ w - \frac{\rho_{wt}(e-e_1)}{\rho_s} - \frac{\rho_{we}(e_1-e_t)}{\rho_s} & (e_t < e_1) \end{cases} \tag{4}$$

The order of pore water discharge in the soil is free water→weakly bound water, →strongly bound water due to varying viscosity. Fig. 6 depicts the relationship between pore water content and time during the consolidation creep in red clay soils, which shows that the type of pore water discharged from the red clay during consolidation creep is mainly free water and weakly bound water, with no discharge of strongly bound water. Most of the free water in the pore space is discharged at the load p=12.5 kPa-400.0 kPa, corresponding to the deformation concentrated in the consolidation stage. The free water in the pore space is discharged when p reaches 800.0 kPa, while the pore water

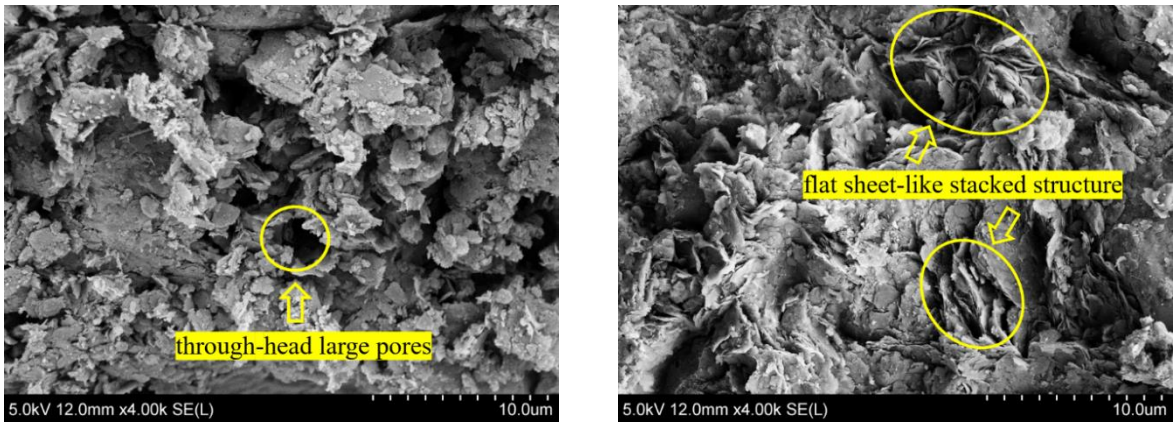

(a) Before solidification creep (b) After solidification creep

Fig. 7 SEM photographs of soil samples before and after consolidation creep

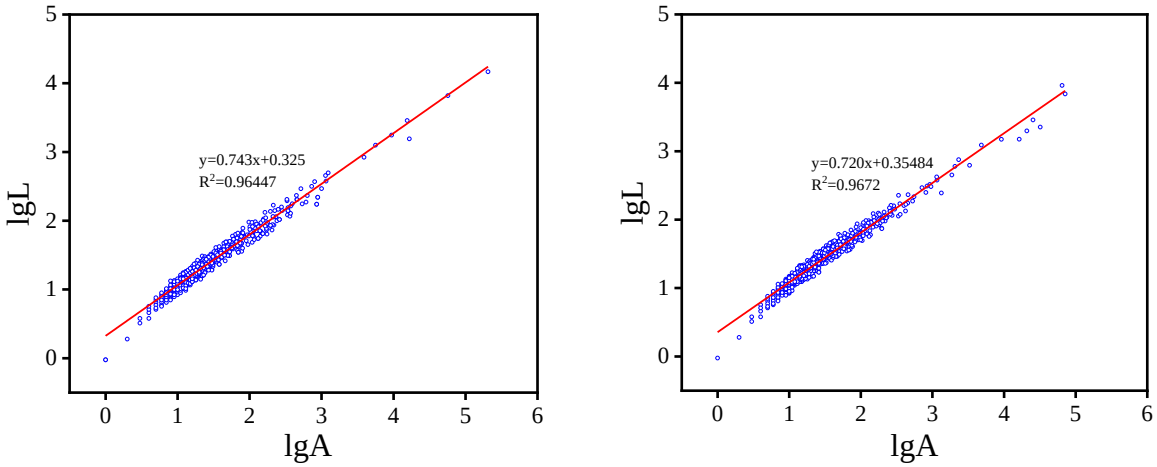

(a) Before solidification creep (b) After solidification creep

Fig. 8 Calculated pore fractal dimension curves before and after solidification creep

pressure is transferred to the skeletal unit body to disorder the initial structure of the soil. The weakly bound water is discharged due to its higher viscosity than the free water when the reduction in w_t has exceeded the total amount of free water contained in the specimen. When the intergranular pressure is high, the weak bound water is extruded, resulting in a higher drainage rate than free water. The high intergranular pressure squeezes out the weakly bound water and rearranges the soil particle units, resulting in narrower pores between the skeletal units. At the end of the test, the free water and most of the weakly bound water in the pores were expelled, with a drop in w_t of 11.51%, by keeping the strongly bound water without discharge. Therefore, it can be concluded that the weakly bound water plays a significant role in the consolidation creep process in red clay.

4. Microstructural changes in red clay

4.1 Scanning electron microscope test results

4.1.1 Qualitative analysis of solidification creep microstructure

The microstructure determines the macro-mechanical characteristics of the soil body. Fig. 7 shows the 4000 times magnification SEM photographs of the specimens before and after the consolidation creep test. Before the consolidation creep test, a granular overhead contact structure is visible with more through-head large pores, and the aggregate is mainly in edge-to-face contact, as shown in Fig. 7(a). In contrast, after the consolidation creep test, the microstructure of red clay evolves into a flat sheet-like stacked structure with fewer large pores and more small pores, and the aggregate is mainly in face-to-face contact, resulting in compressed and compacted soils.

4.1.2 Quantitative analysis of solidification creep microstructure

The fractal dimension D_s may be used to characterize the soil structure complexity directly proportional to each other. The perimeter and area of the pores in the soil can be calculated using Image-Pro Plus image software, while the lgA and lgL scatter plots of the red clay pores before and after the consolidation creep test was generated using Eq. (5). The slope k and correlation coefficient of the fitted straight line was generated by linear fitting of the scatter plots, as shown in Fig. 8. The fractal dimension D_s of the

Table 2 Fractal dimension of pores before and after consolidation creep in red clay

Soil sample status	Before solidification creep	After solidification creep
Slope of the fitted straight line	0.743	0.720
Fractal dimension	1.486	1.440

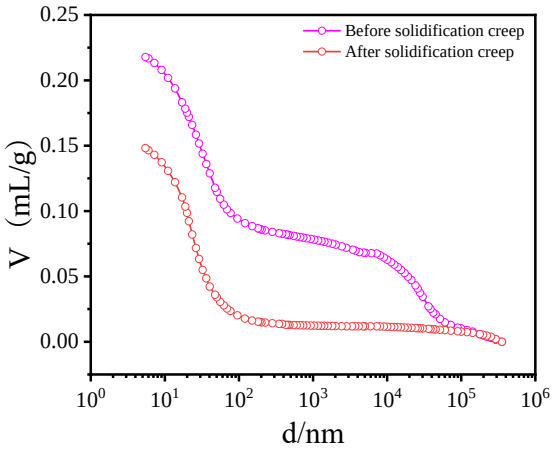

Fig. 9 Cumulative distribution of aperture profiles

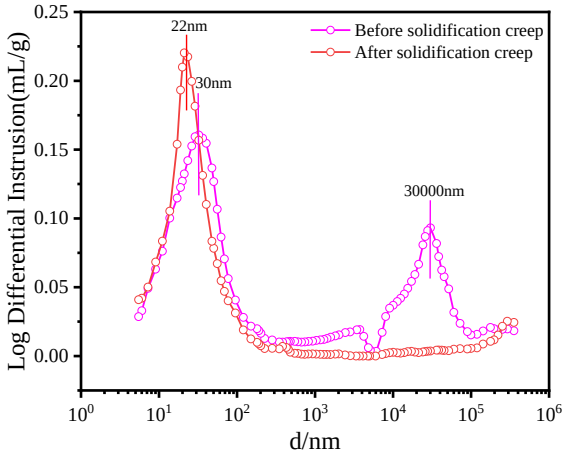

Fig. 10 Aperture distribution graphs

Table 3 Pore size distribution of specimens before and after creep

Specimen	Pore size distribution/%			
	<10 nm	10 nm<100 nm	100 nm <1000 nm	>1000 nm
Before creep	7.33	51.00	5.81	35.86
After creep	11.80	76.25	3.64	8.31

red clay soil before and after consolidation creep tests was computed using D_s=2 k (Chen *et al.* 2020), and the results are shown in Table 2.

$$\lg L = \frac{D_s}{2} + \lg A + C \tag{5}$$

Where, L is the perimeter of the pore, um; A is the area of the pore, um^2; and C is a constant.

Table 2 shows the fractal dimension of the pores of the red clay soil is comparably less after consolidation creep, indicating the simple pore structure of the red clay soil. In contrast, the microstructure of the soil before consolidation creep is a granular overhead contact structure with a large number of large pores. When the soil is exposed to consolidation pressure, the large pores are continuously compressed, resulting in a reduction in larger pores and an increase in smaller pores.

4.2 Results of mercury-pressure tests

Fig. 9 demonstrates the relationship between the pore size and the cumulative volume of mercury pressed into the specimen before and after the creep test. The cumulative volume of mercury pressed into the specimen after creep is comparably lesser than that before creep, indicating a reduction in the pore volume of the specimen and an increase in the compactness after creep.

The pore size distribution of the specimen before and after the creep test is shown in Fig. 10. The pore sizes of the specimen before creep range between 5 nm-100 nm and 7000 nm-100000 nm were distinct bimodal, with the peaks corresponding to a pore size of 30 nm and 30000 nm, respectively. In contrast, the pore sizes of the specimen after creep was 5 nm-100 nm and was single-peaked with a corresponding peak pore size of 22 nm. For the convenience of calculation, the pores are divided into four categories viz., micro-pores, small pores, medium pores, and large pores corresponding to d<10 nm, 10 nm<d<100 nm, 100 nm<d<1000 nm, and d>1000 nm, as shown in Table 3. The pore size of the specimen before creep reaches more than 86% of the total number of pores and the size of pores mostly falls in the intervals 10 nm<d<100 nm and d>1000 nm. However, the pore size distribution of the specimens changed significantly after the creep, more concentrating in the interval of 10 nm<d<100 nm particle size, with a decrease in the number of large and medium pores and an increase in the number of micro-pores and small pores. The specimen before creep has a granular overhead contact microstructure with more through-head large pores and loose soil structure. Further, the soil particles coalesce to form a cohesive body, resulting in a bimodal feature, as seen in the SEM photographs. The soil structure of the specimen is compressed during creep until attaining stability resulting in continuous rearrangement under the action of the load. This causes compression of the large and medium pores of the specimen into small and micropores, resulting in a decrease in the number of large and medium pores and an increase in the number of small and micropores, with a dense soil structure.

The pore is the center of the pore water connection in the soil microstructure. Before consolidation creep, the number of pores of Guilin red clay with sizes d<10 nm and 10 nm<d<100 nm accounts for more than 58% of the total number of pores, and the pores of this size are filled with bonded water. In contrast, free water is mainly distributed in the large and medium pores with d>1000 nm size. The pores with sizes d<10 nm and 10 nm<d<100 nm are more stable than the large and medium pores due to the gravitational force between the particles and can resist

deformation under larger pressure. Before consolidation creep, the Guilin red clay has a granular overhead contact structure with more penetrating overhead macropores. When the soil is under pressure, the discharge of free water starts in large quantities caused by soil pressure resulting in a channel for the discharge of free water offered by the penetrating macropores. The structural connections and big pores are damaged considerably as the pressure rises, while the weakly bound water is expelled, and the creep deformation volume rises. The viscosity of the weakly bound water causes a sluggish discharge process and a long-lasting creep time. Thus, the creep process of Guilin red clay includes the discharge of weakly bound water, with the compression of large and medium pores into small *p* and micropores to transform the soil particles from loose to dense.

5. Conclusions

(1) The Guilin red clay consolidation-creep curve is divided into three stages: decay, initial creep, and stable creep. With *p*=12.5-25.0 kPa, the creep amount is minimal during the decay stage and achieves stability faster. The creep deformation amount increases faster with time during the initial creep stage, with *p*=50.0-400.0 kPa, while creep deformation tends to stabilize with *p*=800.0-1600.0 kPa during the stable creep stage.
(2) In the creep phase of Guilin red clay, free water and weakly bound water are expelled, but the amount of highly bound water remains unchanged. It is primarily the discharge of free water at *p*=12.5 kPa-400.0 kPa, followed by the conversion of weakly bound water to free water at *p*=800.0 kPa-1600.0 kPa. The creep process is the discharge of weakly bound water, the compression of larger pores into small pores, and the conversion of loose soil particles to dense soil particles.
(3) Following creep tests, the microstructure of Guilin red clay changed from a granular overhead contact structure to a flat sheet-like stromatolite structure, resulting in the compression of large and medium pores during consolidation creep and an increase in the number of small and micropores with a decrease in the fractal dimension of the pores.

Acknowledgments

The research described in this paper was financially Supported by National Natural Science Foundation of China (52169022); Hubei Natural Resources Science and Technology Project (ZRZY2022KJ17).

References

An, R., Kong, L., Zhang, X. and Li, C. (2022), "Effects of dry-wet cycles on three-dimensional pore structure and permeability characteristics of granite residual soil using X-ray micro computed tomography", *J. Rock Mech. Geotech. Eng*., **14**(3), 851-860. https://doi.org/10.1016/j.jrmge.2021.10.004.

Bi, G., Ren, C., Xu, H. and Jiang, D. (2022), "Creep behavior of cohesive soils associated with different plasticity indexes", *Environ. Earth Sci*., **81**(5), 1-9. https://doi.org/10.1007/s12665-022-10271-6.

Chen, J.P., Yuan, J., Ye, L.Y. and Peng, Q.W. (2020), "Microstructure change of soft soil under consolidation creep", *Sci. Technol. Eng*., **20**(10), 4087-4094. https://doi.org/10.3969/j.issn.1671-1815.2020.10.044.

Dahhaoui, H., Belayachi, N., Zadjaoui, A. and Nishimura, T. (2022), "One-dimensional compression creep change under temperature and suction effects", *Int. J. Geotech. Eng*., **16**(6), 670-681. https://doi.org/10.1080/19386362.2021.2025306.

Gao, G.R. (2019), *Modern Geotechnics*, Beijing Science Press, Beijing, China.

Ghiyas, S.M.R. and Bagheripour, M.H. (2020), "Stabilization of oily contaminated clay soils using new materials: Micro and macro structural investigation", *Geomech. Eng*., **20**(3), 207-220. https://doi.org/10.12989/gae.2020.20.3.207.

Guo, Y., Ni, W. and Liu, H. (2021), "Effects of dry density and water content on compressibility and shear strength of loess", *Geomech. Eng*., **24**(5), 419-430. https://doi.org/10.12989/gae.2021.24.5.419.

Ibrahim, N., Fayed, A.L., Ahmed, A. and Hammad, M.S. (2022), "Effect of vertical drains and preloading on the creep behavior of soft clay", *Innov. Infrastr. Solut*., **7**(3), 1-12. https://doi.org/10.1007/s41062-022-00780-5.

Jin, P., Zhen, W., Chen, B., Sun, D.a., Gao, Y. and Xiong, Y. (2021), "Effect of microstructure on water retention behavior of lateritic clay over a wide suction range", *Geomech. Eng*., **25**(5), 417-428. https://doi.org/10.12989/gae.2021.25.5.417.

Kaczmarek, Ł. and Dobak, P. (2017), "Contemporary overview of soil creep phenomenon", *Contemp. Trend. Geosci*., **6**, 28-40. https://doi.org/10.1515/ctg-2017-0003.

Kaczmarek, Ł.D., Dobak, P.J. and Kiełbasiński, K. (2017), "Preliminary investigations of creep strain of Neogene clay from Warsaw in drained triaxial tests assisted by computed microtomography", *Studia Geotechnica et Mechanica*, **39**(2), 35-49. https://doi.org/10.1515/sgem-2017-0014.

Kamoun, J. and Bouassida, M. (2018), "Creep behavior of unsaturated cohesive soils subjected to various stress levels", *Arab. J. Geosci*., **11**(4), https://doi.org/10.1007/s12517-12018-13399-12514.

Karim, M.R., Manivannan, G., Gnanendran, C. and Lo, S.R. (2011), "Predicting the long-term performance of a geogrid-reinforced embankment on soft soil using two-dimensional finite element analysis", *Can. Geotech. J*., **48**(5), 741-753. https://doi.org/10.1139/t10-104.

Leoni, M., Karstunen, M. and Vermeer, P. (2008), "Anisotropic creep model for soft soils", *Géotechnique*, **58**(3), 215-226. https://doi.org/10.1680/geot.2008.58.3.215.

Li, J. and Kong, L. (2021), "Creep properties of expansive soils under triaxial drained conditions and its nonlinear constitutive model", *Periodica Polytechnica Civil Eng*., **65**(4), 1269-1278. https://doi.org/10.3311/PPci.18406.

Li, J.X., Wang, C.M. and Zhang, X.W. (2010), "Creep properties and micropore changes of soft soil under different drainage conditions", *Rock Soil. Mech*., **31**(11), 3493-3498. https://doi.org/10.3969/j.issn.1000-7598.2010.11.023.

Liingaard, M., Augustesen, A. and Lade, P.V. (2004), "Characterization of models for time-dependent behavior of soils", *Int. J. Geomech*., **4**(3), 157-177.

Long, Z., Cheng, Y., Yang, G., Yang, D. and Xu, Y. (2021), "Study on triaxial creep test and constitutive model of compacted red clay", *Int. J. Civil Eng*., **19**(5), 517-531. https://doi.org/10.1007/s40999-020-00572-x.

Mesri, G., Febres-Cordero, E., Shields, D. and Castro, A. (1981), "Shear stress-strain-time behaviour of clays", *Geotechnique*,

31(4), 537-552. https://doi.org/10.1680/geot.1981.31.4.537.
MWR (China) (2019), GB/T 50123-2019 Standard for Geotechnical Test Methods. China Planning Press, Beijing, China.
Singh, A. and Mitchell, J.K. (1968), "General stress-strain-time function for soils", *J. Mech. Found. Div*., **94**(1), 21-46. https://doi.org/10.1061/JSFEAQ.0001084.
Tavenas, F., Leroueil, S., Rochelle, P.L. and Roy, M. (1978), "Creep behaviour of an undisturbed lightly overconsolidated clay", *Can. Geotech. J*., **15**(3), 402-423. https://doi.org/10.1139/t78-037.
Wu, F.C. (1984), "Some characteristics of adsorption-bound water measurements and seepage in clayey soils", *Chin. J. Geotech. Eng*., **6**, 84-93.
Xie, G., Deng, M.Y. and Zhang, L. (2013), "A study on the influence of electrolytes on clay bound water", *Dril. Fluid Complet. Fluid*., **30**(6), 1-4.
Zhang, Y., Sha, Y., Chen, J., Gao, B. and Wu, Z. (2019), "Experimental study on creep behavior of red clay of existing foundation in Guiyang City", *Carsologica Sinica*, **38**(4), 627-634.
Zhu, W., Dai, G. and Gong, W. (2021), "Study on cyclic cumulative deformation characteristics and the equivalent cyclic creep model of soft clay", *Math. Prob. Eng*., **2021**, Article ID 5588494. https://doi.org/10.1155/2021/5588494.